Friction model for single-asperity elastic-plastic contacts

Maneesh Mishra, Philip Egberts, Roland Bennewitz, and Izabela Szlufarska

Phys. Rev. B **86**, 045452 — Published 30 July 2012

DOI: 10.1103/PhysRevB.86.045452

Friction model for single asperity elastic-plastic contacts

Maneesh Mishra,[1] Philip Egberts,[2] Roland Bennewitz,[2,*] and Izabela Szlufarska[1,3,†]

[1] *Materials Science Program, University of Wisconsin Madison*
[2] *INM-Leibniz Institute for New Materials, Campus D2 2, 66123 Saarbrücken, Germany*
[3] *Department of Materials Science and Engineering, University of Wisconsin Madison*

(Dated: July 17, 2012)

In this article, we present a new analytical model that describes the plowing coefficient of friction for sliding, elastic-plastic contacts between a conical tip with a spherical extremity and a flat substrate. The model includes the effects of adhesion and bridges the gap between models which are based solely on dislocation activity and those based solely on interfacial effects scaling with the contact area. The DMT approximation for adhesive contact stress is used in our description of the contacts. Our model shows excellent agreement with large scale molecular dynamics simulations and AFM experiments of nanoscratching on copper single crystals. One important result of our study is that the model predicts coefficients of friction that are an order of magnitude higher than typically reported for nanoscale elastic contacts. Furthermore, the coefficients of friction described by the model are very close to values typical of macroscale sliding contacts.

PACS numbers: 68.35.Af,07.05.Tp, 68.37.Ps

I. INTRODUCTION

With the reduction in size of electronic devices to nanometer regime, factors such as the increased adhesive interactions, atomic-scale corrugation, and limited applicability of continuum mechanics approaches limit our ability to design new devices for predictably reliable operation[1]. For example, single-asperity, nanometer-scale friction experiments in the absence of wear typically show very low friction coefficients[1–3]. However, the typical wearless friction coefficients reported in multi-asperity, large scale sliding experiments are approximately one order of magnitude higher[4]. Interestingly, Bowden himself suggested that even in the so-called "wearless" regime in multi-asperity sliding experiments, microscopic damage and plasticity occurs at the length-scale of individual asperities[5]. However, relatively few studies have focused on the understanding of friction in single asperity sliding contacts when wear is observed. For such contacts it has been shown by both molecular dynamics (MD) simulations[6,7] and experiments[8,9] that friction forces and specific mechanisms of deformation are strongly dependent on tip geometry and crystallographic orientation of the sample surface and sliding direction. At relatively low loads, wear can occur by removal of individual atoms from the surface, and atom by atom attrition models have been proposed to explain atomic force microscopy (AFM) experiments in this early stage of wear[10]. While these studies provide useful insights into friction and wear mechanisms at very low normal loads, they do not address the question of how to quantify contributions from plastic deformation to friction in single asperity contacts. Fundamental understanding of single asperity friction for nanoscale elastic-plastic contacts is also required for promising nanolithography techniques using AFM[11]. In addition, with the reduction of contact sizes to the nanometer length scale, adhesive forces between the tip and sample begin to play an increasingly important role[1]. However, there is currently a lack of analytical models for elastic-plastic contacts that can describe the interplay between adhesion and plastic deformation at the sliding interface. Development of such models and understanding of the underlying phenomena are at the forefront of tribological research.

There are two general approaches to modeling friction in the elastic-plastic regime: one based on subsurface dislocation activity[12,13] and the other based on the interfacial contact area[14,15]. Although it is possible to identify the specific mechanisms of dislocation activity during single asperity sliding[16–18], the contact area based approaches are particularly powerful because they are based on geometry of the tip-sample interface and therefore do not require knowledge of mechanisms underlying friction, which can be complicated and are material specific.

In the contact area based approach, the total coefficient of friction (μ_{total}) is decomposed into two components: shear (μ_{S}) and plowing (μ_{P})[14,15]. The shear contribution is related to surface chemistry whereas the plowing contribution is related to plastic deformation of the sample. In this paper, we present a new analytical model for predicting the plowing coefficient of friction for sliding, elastic-plastic contacts that includes adhesive interactions across the sliding interface and a tip geometry that closely matches the typical shape of tips used in AFM experiments. The new model is based on our recently developed formalism for the plowing coefficient of friction for non-adhesive contacts between a spherical asperity and a flat substrate[19]. Here, we first present the derivation of the analytical model by calculating friction forces and normal loads during sliding with elastic and plastic deformation in section II. We have performed MD simulations and AFM experiments to compare with the analytical model; the methods are described in section III. The new analytical model is then validated against MD simulations and AFM scratching experiments on single crystal copper samples in sec-

tion IV.

II. DERIVATION OF THE ANALYTICAL PLOWING MODEL

For non-adhesive contacts, the plowing friction force and normal load for a spherical asperity sliding on a flat surface can be calculated as[19]

$$F_{\text{frictionP}} = p_{\text{m}} A_{\text{Vtotal}}, \tag{1}$$
$$F_{\text{normal}} = p_{\text{m}} A_{\text{Htotal}}, \tag{2}$$

with

$$A_{\text{Vtotal}} = A_{\text{Vep}} + \alpha_{\text{V}} A_{\text{Vpileup}}, \tag{3}$$
$$A_{\text{Htotal}} = A_{\text{Hep}} + \alpha_{\text{H}} A_{\text{Hpileup}}. \tag{4}$$

where A_{Vep} and A_{Hep}, respectively, are the vertical and horizontal projections of the contact area with elastic recovery and no pileup. Correspondingly, A_{Vpileup} and A_{Hpileup} are the vertical and horizontal projections of the pileup area. Parameters α_{H} and α_{V}, respectively, are pre-factors for horizontal and vertical projections of the pileup contact area and represent the distribution of radial stress at the pileup/tip interface[19]. p_{m} is the mean contact pressure at the tip sample interface. This pressure is approximated as being equal to the hardness of the sample for elastic-plastic contacts since the model explicitly assumes that plasticity in the contact is well developed. A_{Vep}, A_{Hep}, A_{Vpileup} and A_{Hpileup} are calculated analytically using the geometry of tip sample interface and are schematically shown in Figures 1(A)-(D).

The contact area projections (eqs. 3-4) are calculated using two physical paramters: elastic recovery and height of pileup. The elastic recovery parameter represents the change in the contact area projections due to recovery of the elastic component of deformation in the back of the sliding tip. The height of the pileup represents the contribution to the contact area projections from the material displaced to the front of the sliding tip. For a detailed derivation of the contributions from these two parameters, see Ref[19]. For calculation of the tip-pileup contact area, the height of the pileup is approximated as

$$h_{\text{pileup}} = \gamma h \left(\frac{A_{\text{Vep}}}{A_{\text{Vp}}}\right), \tag{5}$$

where h is the depth of cut, γ is a fitting parameter, A_{Vep} is the vertical projection of contact area with elastic recovery and A_{Vp} is the vertical projection of contact area assuming no elastic recovery. γ represents the shape of pileup distribution around the sliding tip. Analytical expressions for the contact area projections for a conical tip with a spherical extremity are provided in appendix A.

We estimate the adhesive interactions between the tip and sample using the DMT model[20]. The DMT model assumes that adhesive forces only act in a ring-shaped region outside the actual contact area and the adhesive contact stress is given by the Dugdale approximation[21]

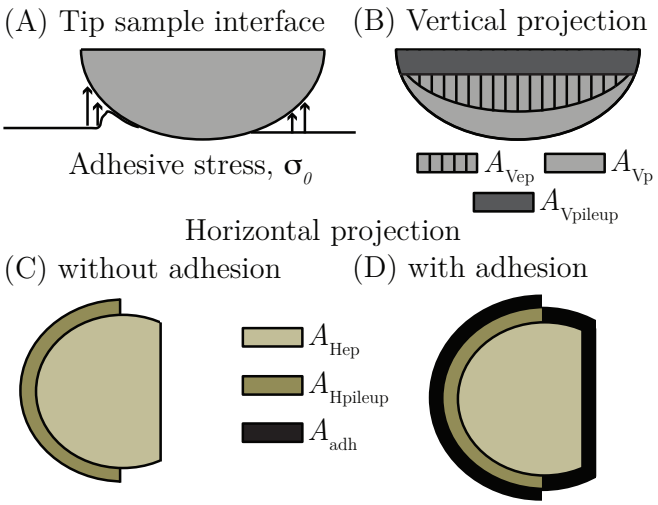

FIG. 1. (Color online) Schematic showing (A) the tip-sample contact interface, (B) vertical projections of contact areas and (C)-(D) horizontal projections of contact area without and with adhesion, respectively.

$$\sigma_0 = \frac{w}{h_0}, \tag{6}$$

where w is the work of adhesion and h_0 is the range of adhesive interactions. The Dugdale approximation assumes a state of constant adhesive stress over a cutoff length h_0 at the gap between a contacting asperity and a flat surface. Figure 1(D) shows the additional ring shaped region on the horizontal contact area projection due to adhesive stresses. The area of adhesive zone, A_{adh}, can be calculated based on geometry of the contact and a derivation of an analytical expression is provided in supplementary materials. The work of adhesion, w, used in our model was measured in AFM experiments and nanoindentation simulations. Specifically, the pull-off force measured during unloading during a normal force versus sample displacement measurement is related to the work of adhesion through

$$F_{\text{pull-off}} = -2\pi w R, \tag{7}$$

where R is the radius of spherical extremity of the conical tip. The range of adhesive interactions used in the Dugdale approximation, h_0, is determined again from nanoindentation simulations by subtracting the tip displacement at zero load from the tip displacement at pull-off during retraction. Once w and h_0 are known, adhesive stress σ_0 is calculated using eq. 6. Using the adhesive stress σ_0 and area of the adhesive zone A_{adh}, the total normal load acting on the sliding tip can be written as[22,23]

$$F_{\text{normal-adh}} = p_{\text{m}} A_{\text{Htotal}} - \sigma_0 A_{\text{adh}}. \tag{8}$$

The plowing coefficient of sliding friction is then calculated as

$$\mu_{\rm P} = \frac{F_{\rm frictionP}}{F_{\rm normal\text{-}adh}} \tag{9}$$

where $F_{\rm frictionP}$ and $F_{\rm normal\text{-}adh}$ are given by eq. 1 and eq. 8, respectively.

III. METHODS

A. MD simulations

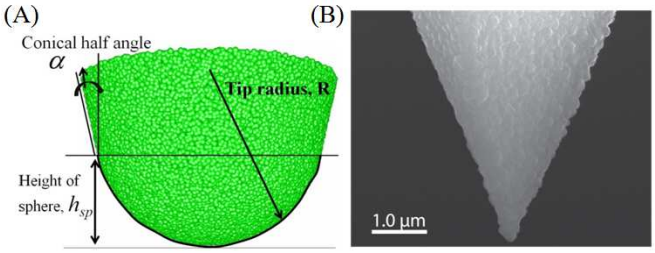

FIG. 2. Sliding tip used in (A) simulations and (B) experiments.

In order to validate our model, we performed large scale MD simulations of single asperity sliding on single crystal copper samples. MD is an excellent tool for testing of the model as the model parameters, such as work of adhesion, can be explicitly specified for the tip-sample interface. Also, by calculating the atomic stress distributions on the tip-sample contact area, plowing contributions to friction can be calculated explicitly and compared to predictions of the analytical model. The interaction potential for Cu is taken from Finnis and Sinclair[24].

Simulations of sliding friction were performed on (110) surface of single crystal copper using a conical tip with spherical asperity as shown in Figure 2(A). The conical half angle is 12° and the radius of spherical extremity R = 10 nm. The tip is made infinitely rigid and the Cu sample has the dimensions $390 \times 350 \times 400$ Å^3. Sliding velocity of 50m/s is used and the temperature of the system is maintained at 300K using Nose-Hoover thermostat[25]. Simulations were carried out at 8 different depths of cut in the range 0.2-3.5 nm. Depth of cut is defined as the distance between the lowest atom in the tip and the average height of the sample surface before deformation.

The pairwise interactions across the tip-sample interface are given by

$$U_{\rm interface} = S\frac{e^{-\kappa r}}{r} - \frac{A}{r^6} \tag{10}$$

where $U_{\rm interface}$ is the interaction energy for atoms interacting across the tip-sample interface and r is the distance between interacting atoms. The first term in eq. 10 represents repulsive interactions where S and κ, respectively, control the magnitude of repulsion and the decay of repulsive interactions. Values of S = 1000 eV Å and κ =3.0 are taken from the study of non-adhesive sliding contacts on Cu[19]. This functional form of repulsive interactions is not unique and it was chosen for computational efficiency. The second term in eq. 10 represents adhesive interactions where A is the coefficient for adhesive van der Waals forces. Several simulations of nanoindentation on Cu sample were perfomed by varying the parameters for adhesive interactions in eq. 10. The largest value of work of adhesion obtained from the nanoindentation simulations is $w = 1.9$ J/m^2 when the interaction parameter for adhesion A =70 eV Å^6. These values of parameters then determined the tip-sample interactions the during sliding simulations.

To calculate the work of adhesion, separate simulations of nanoindentation were performed. The work of adhesion w is calculated by fitting the normal load ($F_{\rm n}$) and contact radius (a) from nanoindentation simulations to the expression[20]

$$F_{\rm n} = \frac{4E_{\rm r}a^3}{3R} - 2\pi R w \tag{11}$$

where R is the radius of the spherical extremity of the conical tip. $E_{\rm r}$ is the reduced Young's modulus for the interface given by the relation $1/E_{\rm r} = (1-\nu_{\rm s}^2)/E_{\rm s} + (1-\nu_{\rm t}^2)/E_{\rm t}$, where $E_{\rm s}$ and $E_{\rm t}$ are the Young's moduli for the sample and the tip, respectively. $\nu_{\rm s}$ and $\nu_{\rm t}$ represent Poisson's ratios for the sample and tip, respectively. Work of adhesion is $w = 1.9$ J/m^2, as obtained from nanoindentation simulations, is used to obtain adhesive stress (σ_0) using eq. 6.

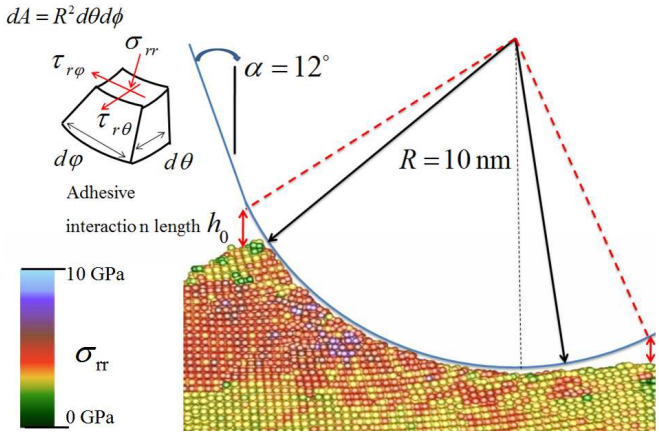

FIG. 3. (Color online) Schematic showing the tip-sample interface with the distribution of radial stress $\sigma_{\rm rr}$ along with the adhesive interaction range h_0. The area element shows the atomic stress tensor on the contact area in the spherical coordinate system. The solid lines show the bounds of interaction without the adhesive forces. The dashed lines show the adhesive interaction forces acting outside the tip-sample contact interface.

The plowing components of friction force and normal load during sliding are calculated directly based on the

distribution of stresses on the contact area in simulations. First, the stress tensor on the contact surface is calculated in the Cartesian xyz coordinate system. The tensor is then transformed to spherical $r\theta\phi$ coordinate system with the origin at the center of the spherical extremity of the sliding tip, as shown in Figure 3. In the spherical coordinate system, contact stresses on the tip-sample contact area are: radial component σ_{rr}, which is perpendicular to the contact interface and shear components $\tau_{r\theta}$ and $\tau_{r\phi}$, which are tangential to the contact interface. The plowing friction force $F_{\text{frictionP}}$ is calculated by projecting the radial force F_{rr} onto the cutting direction, where F_{rr} is obtained by integrating σ_{rr} over the entire contact area. The normal load (F_{n}) is calculated by projecting F_{rr} along the direction normal to the undeformed sample surface. The plowing coefficient of friction μ_{P} is then calculated as the ratio of the plowing friction force and the plowing normal load.

For calculation of shear friction force F_{fs}, the shear friction force F_{s} is projected along the cutting direction where F_{s} is calculated as the vector sum of forces obtained by separately integrating the two shear stresses $\tau_{r\theta}$ and $\tau_{r\phi}$ over the entire contact area. The shear coefficient of friction μ_{s} is calculated as the ratio of the shear friction force and normal load.

B. AFM scratching experiments

To test the applicability of our analytical model for AFM experiments of elastic-plastic sliding friction and wear, we perform wear experiments on oxide-free surfaces of a Cu(100) single crystal using an AFM in ultra-high vacuum (UHV). A diamond coated AFM tip is used for scratching along [100] direction at a velocity of 150 nm/s. A home-built UHV-AFM was used for all experiments discussed in this paper[26]. The AFM operates inside of a commercial UHV chamber produced by Omicron Nanotechnology and is maintained at a pressure of $< 2 \times 10^{-10}$ mbar. Atomically flat Cu(100) surfaces were prepared in the UHV chamber by repeated cycles of argon ion sputtering (1 keV) and annealing (725 K) of a polished (100) face of a Cu single crystal (MaTecK GmbH). The cleaning process resulted in flat terraces up to several 100 nm in width. A stiff, nanocrystalline diamond coated lever with integrated tip (Nanosensors, CDT-NCLR, normal spring constant ∼20-40 N/m) was used in all experiments. These tips, once introduced into the vacuum, were heated at 120°C for 1 hr and then sputtered for 1 min with Ar^+ ions at 1 keV. The stiffness of the cantilevers in both the lateral (twisting) and normal (bending) directions were individually determined by the beam geometry method[27], using the resonant frequency of the first normal bending mode to determine the thickness of the cantilever. Wear scars were created by pressing the cantilever into the surface at constant load. The tip was then moved along the surface, perpendicular to the long axis of the cantilever, for one line in both the forwards and reverse directions. The static bending and twisting signals of the cantilever were measured at a frequency of 8 kHz during scratching. The zero-load force was defined as the deflection measured by the position sensitive detector (PSD) when the tip was out of contact and the cantilever was not bent. Adhesive loads are then a result of the cantilever bending towards the surface, yielding a negative normal force and compressive loads are a result of the cantilever being pushed away from the surface, yielding a positive normal force. Lateral forces are defined as the measured twisting of the cantilever during an experiment. Friction force is defined as the average of the lateral force over forward and backward scan. The surface topography was examined before and after the creation of a wear scar using the non-contact/frequency modulation mode[28]. Switching between non-contact AFM for imaging and contact mode for wear production was automated, such that the rest time of the tip at the beginning and end points of the scratching experiment was minimized. This technique is described in Ref.[18]. During scratching, the sample was moved in the direction parallel to the cantilever beam using the scheme discussed by Cannara *et al.* to remove displacements of the tip relative to the surface with changes in the normal force[29]. This displacement is a result of the 12° angle of the long axis of the cantilever with respect to the sample. AFM images were analyzed with the WSXM software[30].

IV. RESULTS

A. Simulation Results

Figure 4 shows the coefficients of friction determined from sliding simulations. The plowing coefficients of friction from our analytical model (solid line) are calculated using spherical tip radius R =10 nm, conical half angle α =12°, work of adhesion w =1.9 J/m^2, hardness of Cu H = 5.2 GPa and range of adhesive interactions h_0 = 0.3 nm. The specific value of hardness is measured directly from MD and it is determined by the details of MD force field[24]. The excellent agreement between the analytical model and simulation results for plowing coefficients of friction (Figure 4) demonstrates the validity of our analytical model for single asperity adhesive contacts. It is interesting to note from Figure 4 that for normal loads higher than a crtical load ($F_{\text{n}} > 160$ nN), plowing is the dominant contribution to total coefficient of friction and $\mu_{\text{shear}} << \mu_{\text{P}}$. Specifically, we found that for $F_{\text{n}} > 160$ nN, $\mu_{\text{shear}} = 0.046 \pm 0.02$. This value for shear coefficient of friction will be used later to compare with experimental results from AFM nanoscratching, where plowing and shear contributions to coefficient of friction cannot be calculated separately. For normal loads below the critical load ($F_{\text{n}} < 160$ nN), deformation is primarily elastic with a small contribution from plastic deformation and thus the plowing model, which assumes plasticity to

be fully developed, shows deviations from the simulation results for the plowing coefficient of friction.

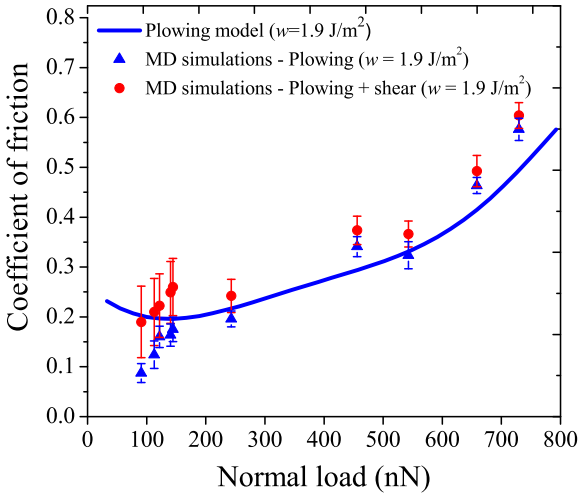

FIG. 4. Coefficient of friction as a function of normal load from simulations. Total coefficients of friction (circles) and plowing coefficients of friction (triangles) are shown along with results from analytical model (solid line).

B. Experimental Results

Figure 5 (A) shows the surface approximately 12 hrs after sputter cleaning the surface. Flat terraces of several 100 nm can be clearly observed, where individual terraces are separated in height by one atomic layer, or 1.8 Å. A white arrow marks a reference topographic feature on the surface located on a large terrace. This area was chosen as the scratching site due to the low number of defects on this terrace and the large atomically flat area. Following scratching, a wear scar is observed in Figure 5 (B), as well as the same reference topographic feature, highlighted by the white arrow. At the site where the surface has been scratched, copper has been displaced. In the copper terraces surrounding the scratch site, no change in any of the topographic features has occurred. Therefore, it is likely that subsurface dislocations have been nucleated, but they have not reached the surface, and are therefore not visible in topographic images of the scratch. This result is in contrast to AFM-based indentation studies on Cu(100)[31] and nanoscratching studies of KBr(100)[18], where topographic evidence of dislocation activity has been shown. The lateral force measured during scratching is shown in Figure 5 (C), indicating is significant frictional dissipation. The friction coefficient measured in Figure 5 (C) was 0.42 ± 0.06, in contrast to the result of Gosvami *et al.*, who measured a friction coefficient on Cu(100) of 0.004 ± 0.001 before the onset of wear[32].

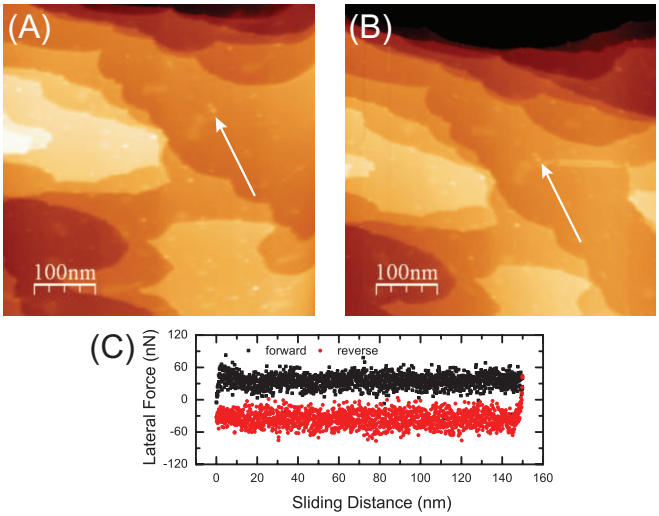

FIG. 5. (Color online) AFM topographic images of the Cu(100) surface (A) directly before scratching and (B) after with the same Z-height scale. The scratch shown in (B) corresponds to the lowest normal load, which is 78 nN. Image (A) and (B) were acquired at a rotation angle of 90° to better acquire the topographic image of the scratch, and have been rotated back to 0° in the processed image shown here. An arrow is pointing to a surface defect near the beginning point of the scratch in both the before and after images. The step height between each atomic terrace corresponds represents a single atomic step or 1.8 Å. (C) Lateral force data in the forwards (left to right) and reverse (right to left) sliding directions acquired during scratching.

C. Comparison between Experiment and Simulation

Figure 6 shows the results of both the AFM scratch experiments and the analytical model. For the model, we use $R = 12$ nm and the AFM conical half angle α =22°, measured from tip images acquired in the scanning electron microscope. A work of adhesion of w =3.1 J/m^2 is calculated using the DMT model based on the pull-off force measured in AFM experiments. Hardness of Cu is taken as H = 3.5 GPa[33] and range of adhesive interactions is $h_0 = 0.3$ nm (the same as in MD simulations). The total coefficients of friction calculated from experiments (squares) show an excellent agreement with our analytical model. It should be noted that the experimental Cu samples have a lower hardness value than used in the MD simulations. Consequently plasticity is well developed at lower normal loads, where the the MD simulations begin to deviate. As a result, the analytical model shows agreement with experimental results even for low normal loads.

Further comparison between simulation and experiment scratching experiments is provided in Figure 7. Figure 7 (A) and (C) show the surface topography in simulation and experiment after scratching. Both scratches are performed at similar normal loads, and show a simi-

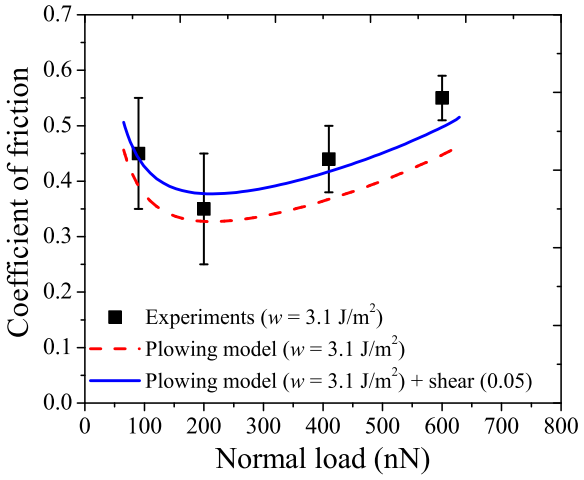

FIG. 6. Total coefficient of friction (filled squares) from AFM experiments plotted as a function of normal load during sliding. Also shown are plowing (dashed line) and total (solid line) coefficients of friction calculated using the model with work of adhesion = 3.1 J/m^2. Shear coefficient of friction is assumed to be 0.05 as calculated from simulations for normal load in the range 160-730 nN. Error bars in the experimental results indicate the standard deviation of the measured mean friction.

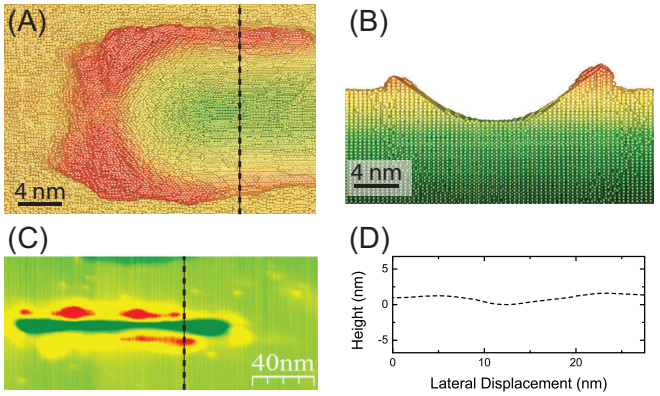

FIG. 7. (Color online) Topographic image of a simulated scratch (A) on copper. In (A), the surface was scratched at a normal load of 658 nN. A profile (B) of the section marked by the dashed line in (A) shows in more detail, the depth of the scratch. Experimental topographic image (C) of a scratch. In (C), the surface was scratched at a normal load of 587 nN. (D) Line profile of the topographic image indicated with a black line in (C) with the same scale as (B).

lar scratch grove width. Furthermore, the overall shape of the scratch and the pileup surrounding the scratch is similar in both simulation and experiment. Closer examination of Figures 7 (B) and (D) show that the depth of the scratch in the experimental results is smaller. One complication of the experimental multi-mode approach in determining the scratch depth, since the same tip was used to both scratch the surface and then subsequently image the scratch. A result of this procedure is a strong tip convolution in topographic images when imaging the scratched region. In addition, the long range attractive forces measured in non-contact AFM imaging[28] further complicate image reconstruction and limit the accuracy of the scratch depth measurement. The tip convolution effect leads to an under-estimation of the scratch depth and consequently experimental images provide a lower bound for the scratch depth. On the other hand, the experimental procedure used in this study provides a good estimate of the pileup height surrounding the scratch. It is therefore somewhat surprising that pileup height calculated from experiments and MD exhibit deviations, as shown in Figure 7 (B) and (D). Specifically, the simulation results show a pileup height of 3-4 copper atoms (or 5.4-7.2 Å) compared to the typical pileup of 1-2 atoms (1.8-3.6 Å) in experiment. A possible source of the discrepancy in pile-up height may stem from the different time scales involved in AFM experiments and MD simulations. In AFM, topographic images are acquired on the time scales of hours after the scratch has been performed, and in this case ∼0.5 hrs for the first image to be acquired. It has been reported that on these time scales a significant diffusion of evaporated copper atoms on copper surfaces is expected[34]. It is likely that similar high diffusion rates of the copper atoms in the pileup may occur after scratching. However, in simulation, the topographic images are acquired within 25-30 ps of scratching the site. At this time scale, there is not sufficient time for diffusion processes to occur. The effect of diffusion is further visible in the comparison between simulation and experiment as the pileup in experiments typically extends further laterally from the scratch site itself in comparison with the simulated scratch.

V. DISCUSSION

The comparison with experimental and MD results demonstrates that our analytical model for single asperity elastic-plastic sliding can describe the coefficient of plowing friction in presence of adhesion. It is interesting to note that the position of the minimum in the μ_P vs. F_n plot (Figure 6) is controlled by relative contributions to friction from adhesive and plowing forces. In the DMT theory[20], used to describe adhesive interactions in our model, the adhesive zone is a ring-shaped area outside the tip-sample contact area. As the normal load decreases, the area of the adhesive zone becomes larger relative to the total horizontal contact area and adhesive forces dominate the contribution to μ_P. At larger loads, an increase in the pileup height increases the contribution to friction from deformation, which eventually becomes the dominant contribution to μ_P. Since adhesion controls μ_P at low loads, a large value of work of adhesion will shift the minima to larger loads. This observation is

consistent with our results (Figure 4 and Figure 6) where a higher value of work of adhesion in experiments shifts the minima in the μ_P vs. F_n plot towards higher normal loads as compared to simulations.

In order to include the effects of pileup and adhesive interactions on coefficient of friction, the analytical model introduces two parameters: γ (eq. 5) and h_0 (eq. 6). The fitting parameter (γ) represents the shape of the pileup in contact with the sliding tip. A large value of γ is obtained when a significant fraction of the displaced material is in front of the sliding tip whereas a small value of γ is obtained when a large fraction of the displaced material moves to the side of the sliding tip[19]. Thus γ is a material specific parameter and is also dependent on the direction of sliding on crystalline surfaces[19].

The agreement of the analytical model with the experimental results is independent of the choice of the model parameter h_0. The range of adhesive interactions h_0 determines the adhesive stresses and the area of adhesive zone (given by eq. 6). A larger value of h_0 increases the area of adhesive contact and decreases the adhesive stress. Thus the choice of h_0 has a small effect on the final results of the model for a given work of adhesion value as shown in fig. 8.

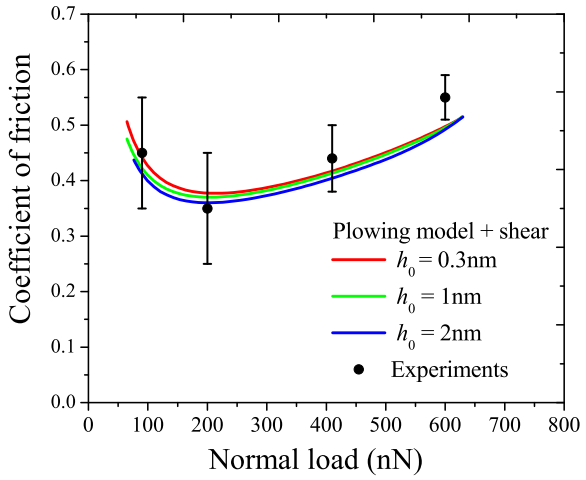

FIG. 8. (Color online) Results of the analytical model for three different values of h_0 along with the results from AFM experiments. Work of adhesion w=3.1 J/m^2 is used for all three cases.

An important observation from Figure 4 and Figure 6 is that the coefficients of friction for single asperity elastic-plastic contacts are an order of magnitude higher than for elastic contacts on Cu[3]. This increase in the coefficient of friction due to plastic deformation and wear observed in experiments confirms findings from our simulations that $\mu_S << \mu_P$. Interestingly, in presence of plastic deformation and wear, the nanoscale coefficients of friction for Cu are comparable to values typical of macroscale contacts $(0.4 - 0.9)$[35,36].

VI. CONCLUSIONS

We have developed an analytical model for elastic-plastic friction in the presence of adhesion and for parameters relevant to AFM experiments. The plowing coefficient of friction is modeled as the ratio of vertical and horizontal projections of contact area between a conical tip with a spherical extremity and a flat surface. The model is validated against the plowing coefficients of friction calculated from MD simulations of sliding friction on crystalline Cu. For conditions of fully developed plasticity under the sliding tip, plowing is shown to be the dominant contribution to friction and $\mu_{shear} << \mu_P$. The model shows excellent agreement with the coefficients of friction from AFM nanoscratching experiments on single crystal Cu. Our new model is the first analytical model that can describe the interplay between adhesive forces at the interface and subsurface plastic deformation for single asperity sliding contacts.

ACKNOWLEDGEMENTS

I. S. and M. M. acknowledge support from NSF grant CMMI-0747661. Use of the Center for Nanoscale Materials was supported by the U. S. Department of Energy, Office of Science, Office of Basic Energy Sciences, under Contract No. DE-AC02-06CH11357. R. B. and P. E. acknowledge Eduard Arzt for the support and N.N. Gosvami for SEM imaging of the AFM tip.

Appendix A: Contact stresses and contact area projections for a conical tip with spherical asperity

In order to evaluate the friction force and the normal load using eqs. 1-8 , one needs to calculate the contact area projections of the tip sample interface and stress distribution on the contact area interface. The AFM sliding tip can be modeled as a conical tip with a spherical asperity as shown in Figure 2. The contact stress on the elastic plastic contact area projections (A_{Vep} and A_{Hep}) can be approximated by hardness of the sample which is H = 5.2 GPa as obtained from simulations and is comparable to experimental results for Cu[33]. As shown in Ref[19], the contact radial stress on the pileup surface can be approximated as a linear function that decreases from the value of hardness at the sample surface to zero on the top of the pileup-tip contact area. For the calculation of parameters α_H and α_V for a spherical tip, see Ref[19]. For the conical part of the tip, α_H=0.5 and α_V=0.5.

For a conical tip with a spherical extremity sliding on a flat sample, the expressions for contact area projections are given below. The exact expressions for contact areas depend on whether the sample surface is in contact with only the spherical extremity or with both the spherical and conical surfaces of the sliding tip.

The vertical projection of contact area of elastic plastic contact is written as

$$A_{\mathrm{Vep}} = \begin{cases} \rho^2 \sin^{-1}(a_{\mathrm{r}}/\rho) - a_{\mathrm{r}}\sqrt{\rho^2 - a_{\mathrm{r}}^2} & \text{if } h \le h_{\mathrm{sp}} \\ \rho^2 \sin^{-1}(a_{\mathrm{r}}/\rho) - a_{\mathrm{r}}\sqrt{\rho^2 - a_{\mathrm{r}}^2} & \\ +(h - h_{\mathrm{sp}})^2 \tan\alpha & \text{if } h > h_{\mathrm{sp}} \\ +(h - h_{\mathrm{sp}})a_{\mathrm{sp}} & \end{cases} \quad \text{(A1)}$$

where h_{sp} is the height of the spherical extremity (Figure1 in the main text) and $a_{\mathrm{sp}} = \sqrt{(2Rh_{\mathrm{sp}} - h_{\mathrm{sp}}^2)}$. h is the depth of cut, α is the conical half angle, R is the radius of the spherical extremity, $a_{\mathrm{r}} = a\cos\omega$ and ω is the elastic recovery angle. ω is the angle made by the elastically recovered contact area at the back of the sliding tip. For a detailed derivation of elastic recovery angle ω using tip geometry and hardness of the sample, see Ref.[19]. In eq. A1, ρ and contact radius a can be written as:

$$\rho = \begin{cases} \sqrt{(R^2 - a^2\sin^2\omega)} & \text{if } h \le h_{\mathrm{sp}} \\ \sqrt{(R^2 - a_{\mathrm{sp}}^2\sin^2\omega)} & \text{if } h > h_{\mathrm{sp}}\ . \end{cases} \quad \text{(A2)}$$

and

$$a = \begin{cases} \sqrt{(2Rh - h^2)} & \text{if } h \le h_{\mathrm{sp}} \\ a_{\mathrm{sp}} + (h - h_{\mathrm{sp}})\tan\alpha & \text{if } h > h_{\mathrm{sp}} \end{cases} \quad \text{(A3)}$$

Horizontal projection of contact area of elastic plastic contact can be written as

$$A_{\mathrm{Hep}} = 0.5a^2(\pi + 2\omega + \sin(2\omega)) \quad \text{(A4)}$$

where a is calculated using eq. A3.

Similarly, as the expressions for A_{Vep} and A_{Hep} (eq. A1 and A4, respectively), the expressions for projections of tip-pileup contact area depend on whether the pileup in front of the sliding is in contact with the spherical surface, conical surface or both the conical and spherical surfaces of the tip. If average height of the pileup h_{pileup} (see Ref.[19]) is known, vertical projection of tip-pileup contact area is given by:

if $(h + h_{\mathrm{pileup}}) \le h_{\mathrm{sp}}$

$$A_{\mathrm{Vpileup}} = R^2\sin^{-1}(a_p^2/R) - a_p\sqrt{(R^2 - a_p^2)} - R^2\sin^{-1}(a^2/R) - a\sqrt{(R^2 - a^2)} \quad \text{(A5)}$$

where a_p is the contact radius with pileup given as:

$$a_{\mathrm{p}} = \begin{cases} \sqrt{2R(h + h_{\mathrm{pileup}}) - (h + h_{\mathrm{pileup}})^2} & \text{if } h \le h_{\mathrm{sp}} \\ a_{\mathrm{sp}} + (h + h_{\mathrm{pileup}} - h_{\mathrm{sp}})\tan\alpha & \text{if } h > h_{\mathrm{sp}} \end{cases} \quad \text{(A6)}$$

and if $h \le h_{\mathrm{sp}}$ and $(h + h_{\mathrm{pileup}}) > h_{\mathrm{sp}}$

$$A_{\mathrm{Vpileup}} = R^2\sin^{-1}(a_{\mathrm{ap}}^2/R) - a_{\mathrm{ap}}\sqrt{(R^2 - a_{\mathrm{ap}}^2)} - R^2\sin^{-1}(a^2/R) - a\sqrt{(R^2 - a^2)} + (h + h_{\mathrm{pileup}} - h_{\mathrm{sp}})a_{\mathrm{sp}} + (h + h_{\mathrm{pileup}} - h_{\mathrm{sp}})^2\tan\alpha \quad \text{(A7)}$$

and if $h \ge h_{\mathrm{sp}}$

$$A_{\mathrm{Vpileup}} = (h + h_{\mathrm{pileup}} - h_{\mathrm{sp}})a_{\mathrm{sp}} + (h + h_{\mathrm{pileup}} - h_{\mathrm{sp}})^2\tan\alpha. \quad \text{(A8)}$$

The horizontal projection of pileup area is written as:

$$A_{\mathrm{Hpileup}} = 0.5\pi(a_{\mathrm{p}}^2 - a^2) \quad \text{(A9)}$$

where a and a_{p} are given by eq. A3 and A6, respectively.

Similarly as the pileup contact areas (eq. A5 and eqs. A7-A9), the horizontal projection of adhesive contact area also depends on whether the sample is in adhesive contact with conical or spherical part of the sliding tip. The total adhesive contact area can be written as

$$A_{\mathrm{adh}} = A_{\text{adh-front}} + A_{\text{adh-back}} \quad \text{(A10)}$$

where $A_{\text{adh-front}}$ and $A_{\text{adh-back}}$, respectively, represent adhesive contact area in front and back of the sliding tip. For adhesive interaction range h_0, adhesive contact area in front is given as:

if $(h + h_{\mathrm{pileup}} + h_0) \le h_{\mathrm{sp}}$

$$A_{\text{adh-front}} = 0.5\pi\{2R(h + h_{\mathrm{pileup}} + h_0) - (h + h_{\mathrm{pileup}} + h_0)^2 - a_{\mathrm{p}}^2\}, \quad \text{(A11)}$$

if $(h + h_{\mathrm{pileup}} + h_0) > h_{\mathrm{sp}}$ and $(h + h_{\mathrm{pileup}}) < h_{\mathrm{sp}}$

$$A_{\text{adh-front}} = 0.5\pi\{[a_{\mathrm{sp}} + (h + h_{\mathrm{pileup}} + h_0 - h_{\mathrm{sp}})\tan\alpha]^2 - a_{\mathrm{p}}^2\}. \quad \text{(A12)}$$

and if $(h + h_{\mathrm{pileup}}) \ge h_{\mathrm{sp}}$

$$A_{\text{adh-front}} = 0.5\pi\{[a_{\mathrm{sp}} + (h + h_{\mathrm{pileup}} + h_0 - h_{\mathrm{sp}})\tan\alpha]^2 - [a_{\mathrm{sp}} + (h + h_{\mathrm{pileup}} - h_{\mathrm{sp}})\tan\alpha]^2\}. \quad \text{(A13)}$$

The adhesive contact area in the back is given as,

if $(h + h_0) \le h_{\mathrm{sp}}$

$$A_{\text{adh-back}} = 0.5(2\omega + \sin(2\omega)) \{\ 2R(h + h_0) - (h + h_0)^2 - a^2\},$$

if $(h + h_0) > h_{\mathrm{sp}}$ and $h < h_{\mathrm{sp}}$

$$A_{\text{adh-back}} = 0.5(2\omega + \sin(2\omega)) \{[a_{\mathrm{sp}} + (h + h_0 - h_{\mathrm{sp}})\tan\alpha]^2 - a^2\}, \quad \text{(A14)}$$

and if $h \ge h_{\mathrm{sp}}$

$$A_{\text{adh-back}} = 0.5(2\omega + \sin(2\omega)) \{\ [a_{\mathrm{sp}} + (h + h_0 - h_{\mathrm{sp}})\tan\alpha]^2 - [a_{\mathrm{sp}} + (h - h_{\mathrm{sp}})\tan\alpha]^2\}. \quad \text{(A15)}$$

* Roland.Bennewitz@inm-gmbh.de
† szlufarska@wisc.edu

[1] I. Szlufarska, M. Chandross, and R. W. Carpick, J. Phys. D: Appl. Phys. **41**, 123001 (2008).
[2] Y. Mo, K. T. Turner, and I. Szlufarska, Nature **457**, 1116 (2009).
[3] N. N. Gosvami, T. Filleter, P. Egberts, and R. Bennewitz, Tribol. Lett. **39**, 19 (2010).
[4] F. P. Bowden and L. Leben, P. Roy. Soc. Lond. A. Mat. **169**, 371 (1939).
[5] F. P. Bowden and D. Tabor, in *The Friction and Lubrication of Solids* (Oxford University Press, New York, 1986) pp. 73–89.
[6] J. J. Zhang, T. Sun, Y. D. Yan, Y. C. Liang, and S. Dong, App. Surf. Sci. **254**, 4774 (2008).
[7] R. Komanduri and L. M. Raff, P. I. Mech. Eng. B-J. Eng. **215**, 1639 (2001).
[8] A. A. Tseng, C.-F. J. Kuo, S. Jou, S. Nishimura, and J.-i. Shirakashi, Appl. Surf. Sci. **257**, 9243 (2011).
[9] B. L. Lawson, N. Kota, and O. B. Ozdoganlar, J. Manuf. Sci. E.-T. ASME **130**, 031116 (2008).
[10] H. Bhaskaran, B. Gotsmann, A. Sebastian, U. Drechsler, M. A. Lantz, M. Despont, P. Jaroenapibal, R. W. Carpick, Y. Chen, and K. Sridharan, Nature Nanotech. **5**, 181 (2010).
[11] A. A. Tseng, Nano Today **6**, 493 (2011).
[12] A. M'ndange-Pfupfu and L. D. Marks, Tribol. Lett. **39**, 163 (2010).
[13] B. Bhushan and M. Nosonovsky, Acta Mater. **52**, 2461 (2004).
[14] S. Lafaye, C. Gauthier, and R. Schirrer, Tribol. Lett. **21**, 95 (2006).
[15] J. Goddard and H. Wilman, Wear **5**, 114 (1962).
[16] R. Bennewitz and J. T. Dickinson, MRS Bulletin **33**, 1174 (2008).
[17] D. Mulliah, S. D Kenny, E. Mcgee, R. Smith, A. Richter, and B. Wolf, Nanotechnology **17**, 1807 (2006).
[18] P. Egberts and R. Bennewitz, Adv. Sci. Tech. **64**, 25 (2010).
[19] M. Mishra and I. Szlufarska, Tribol. Lett. **45**, 417 (2012).
[20] B. Derjaguin, J. Colloid Interface Sci. **53**, 314 (1975).
[21] D. Maugis, J. Colloid Interface Sci. **150**, 243 (1992).
[22] W. R. Chang, I. Etsion, and D. B. Bogy, J. Tribol. **110**, 57 (1988).
[23] Z. Liu, J. Sun, and W. Shen, Tribology International **35**, 511 (2002).
[24] M. W. Finnis and J. E. Sinclair, Philos. Mag. A **50**, 45 (1984).
[25] W. Shinoda, M. Shiga, and M. Mikami, Phys. Rev. B **69**, 134103 (2004).
[26] L. Howard, E. Meyer, R. Lüthi, H. Haefke, R. Overney, H. Rudin, and H.-J. Güntherodt, Applied Physics Letters **63**, 117 (1993).
[27] E. Meyer, H. J. Hug, and R. Bennewitz, *Scanning Probe Microscopy: The Lab on a Tip* (Springer-Verlag, Berlin, 2004).
[28] S. Morita, R. Wiesendanger, and E. Meyer, eds., *Noncontact Atomic Force Microscopy*, NanoScience And Technology (Springer-Verlag, Berlin, 2002).
[29] R. J. Cannara, M. J. Brukman, and R. W. Carpick, Review of Scientific Instruments **76**, 053706 (2005).
[30] I. Horcas, R. Fernández, J. M. Gómez-Rodríguez, J. Colchero, J. Gómez-Herrero, and A. M. Baro, Review of Scientific Instruments **78**, 013705 (2007).
[31] T. Filleter and R. Bennewitz, Nanotechnology **18**, 044004 (2007).
[32] N. N. Gosvami, T. Filleter, P. Egberts, and R. Bennewitz, Tribology Letters **39**, 19 (2010).
[33] R.-C. Chang, F.-Y. Chen, and C.-E. Sun, Key Eng. Mat. **326**, 357 (2006).
[34] C. Klünker, J. Hannon, M. Giesen, H. Ibach, G. Boisvert, and L. Lewis, Physical Review B **58**, 7556 (1998).
[35] E. Marui and H. Endo, Wear **249**, 582 (2001).
[36] Y. S. Zhang, Z. Han, K. Wang, and K. Lu, Wear **260**, 942 (2006).